Published OnlineFirst July 17, 2012; DOI: 10.1158/1078-0432.CCR-12-1379

Cancer Therapy: Preclinical

Clinical Cancer Research

Biomarker and Pharmacologic Evaluation of the γ-Secretase Inhibitor PF-03084014 in Breast Cancer Models

Cathy C. Zhang[1], Adam Pavlicek[1], Qin Zhang[1], Maruja E. Lira[1], Cory L. Painter[1], Zhengming Yan[1], Xianxian Zheng[1], Nathan V. Lee[1], Mark Ozeck[1], Ming Qiu[1], Qing Zong[2], Patrick B. Lappin[2], Anthony Wong[2], Paul A. Rejto[1], Tod Smeal[1], and James G. Christensen[1]

Abstract

Purpose: We aimed to assess the biologic activity of PF-03084014 in breast xenograft models. The biomarkers for mechanism and patient stratification were also explored.

Experimental Design: The *in vitro* and *in vivo* properties of PF-03084014 were investigated. The mRNA expressions of 40 key Notch pathway genes at baseline or after treatment were analyzed to link with the antitumor efficacy of PF-03084014 in a panel of breast cancer xenograft models.

Results: *In vitro*, PF-03084014 exhibited activity against tumor cell migration, endothelial cell tube formation, and mammosphere formation. *In vivo*, we observed apoptosis, antiproliferation, reduced tumor cell self-renewal ability, impaired tumor vasculature, and decreased metastasis activity after the treatment of PF-03084014. PF-03084014 treatment displayed significant antitumor activity in 10 of the 18 breast xenograft models. However, the antitumor efficacy in most models did not correlate with the *in vitro* antiproliferation results in the corresponding cell lines, suggesting the critical involvement of tumor microenvironment during Notch activation. In the tested breast xenograft models, the baseline expressions of the Notch receptors, ligands, and the cleaved Notch1 failed to predict the antitumor response to PF-03084014, whereas several Notch pathway target genes, including *HEY2*, *HES4*, and *HES3*, strongly corresponded with the response with a *P* value less than 0.01. Many of the best molecular predictors of response were also significantly modulated following PF-03084014 treatment.

Conclusions: PF-03084014 showed antitumor and antimetastatic properties via pleiotropic mechanisms. The Notch pathway downstream genes may be used to predict the antitumor activity of PF-03084014 and enrich for responders among breast cancer patients. *Clin Cancer Res; 1–12. ©2012 AACR.*

Introduction

In mammalian cells, Notch signaling is activated when the Notch family receptors (Notch1–4) bind to the membrane-bound ligands (Jagged1, Jagged2, Delta-like1, Delta-like3, and Delta-like4) on neighboring cells. Upon ligand binding, the Notch receptor undergoes a series of proteolytic cleavage steps. The constitutively active γ-secretase complex catalyzes the final step, which results in the release of the Notch intracellular domain (NICD). The NICD subsequently translocates to the nucleus, where it acts as a transcriptional coactivator of the Notch target genes. In human breast cancers, aberrant Notch signaling has been reported to promote disease progression and is associated with significantly poor overall survival (1, 2). Notch1 and Notch2 fusion proteins have been recently reported in breast cancer cell lines and patient specimens (3), and the treatment of breast cancer cell lines that harbor these fusions with the γ-secretase inhibitor (GSI), DAPT, have shown robust growth inhibition when the γ-secretase cleavage site is present. NUMB, a negative regulator of the Notch signaling, is lost in approximately 50% of human mammary carcinomas, and its expression is inversely correlated with tumor grade and proliferation rate (4). Notch signaling also drives cancer progression via cross-talk with many other oncogenic pathways, such as EGF receptor and TGFβ signaling (5, 6).

During malignant progression, Notch signaling affects a broad range of the cellular activities of tumor cells and their microenvironment, including cell proliferation, differentiation, apoptosis, angiogenesis, and invasion (5–7). Notch is also known for the maintenance and survival of

Authors' Affiliations: [1]Oncology Research Unit and [2]Drug Safety, Pfizer Global Research and Development, La Jolla, California

Note: Supplementary data for this article are available at Clinical Cancer Research Online (http://clincancerres.aacrjournals.org/).

C.C. Zhang and A. Pavlicek contributed equally as first authors.

Corresponding Authors: Cathy C. Zhang, Pfizer Oncology, 10724 Science Center Rd. (CB3), La Jolla, CA 92121. Phone: 858- 622-3125; Fax: 858-622-5999; E-mail: cathy.zhang@pfizer.com; and Adam Pavlicek, Regulus Therapeutics, 3545 John Hopkins Court, San Diego, CA 92129. Phone: 858-202-6343; E-mail: apavlicek@regulusRx.com

doi: 10.1158/1078-0432.CCR-12-1379

Published OnlineFirst July 17, 2012; DOI: 10.1158/1078-0432.CCR-12-1379

Translational Relevance

Aberrant Notch signaling, which requires the constitutive activation of γ-secretase, is implicated in the disease progression of breast cancer. PF-03084014 is a small molecule γ-secretase inhibitor that is currently under phase I clinical investigation. To aid the clinical development of PF-03084014 in breast cancer, we characterized the diverse biologic properties of PF-03084014 and evaluated the biomarkers in the preclinical setting. By impairing Notch signaling, PF-03084014 showed significant antitumor efficacy in a subset of breast cancer xenograft models via various mechanisms, such as apoptosis induction, the inhibition of cancer stem cell self-renewal, antiproliferation, and antiangiogenesis. The Notch pathway target gene expressions correlated with the antitumor efficacy and can potentially serve as biomarkers for proof-of-mechanism and patient enrichment. This work provides guidance for the clinical investigation of PF-03084014 therapy for breast cancer patients.

tumor-initiating cells. Notch signaling directs endothelial cell fate during new vessel formation via the Notch ligands Dll4 and Jag1 (8, 9), thereby mediating tumor angiogenesis, progression, and metastasis. Notch signaling is also triggered when tumor cells interact with neighboring endothelial cells and promote neovascularization (10). In stromal cells, in which Notch receptors and ligands are expressed (11), Notch signaling regulates cell migration and controls smooth muscle cell growth and apoptosis (12). Elevated expression levels of Jagged1 promote the spread of breast cancer cells to the bone by activating stromal cell Notch signaling (13). These findings highlight the critical role that of Notch signaling plays in tumor–stromal cell communication during solid tumor disease progression and suggest that therapeutic assessment of a Notch inhibitor should involve both the tumor cells and the corresponding microenvironment.

The complexity of Notch pathway activation during cancer development provides numerous opportunities for the development of targeted therapies; several proteins involved in the Notch signaling pathway are therapeutic targets for the treatment of various types of cancers (14), including anti-Dll4 antibodies (15) and γ-GSIs (16, 17). PF-03084014 is a potent and selective GSI, which is currently under clinical phase I development. By blocking Notch signaling, PF-03084014 exhibited antitumor efficacy in human T-ALL xenograft models (18). In this article, we evaluated the pharmacologic properties of PF-03084014 in breast cancer xenograft models and investigated the candidate biomarkers.

Materials and Methods

All cell lines and fine chemicals were purchased from American Type Culture Collection and Sigma-Aldrich, respectively, unless noted otherwise. MDA-MB-231Luc was purchased from Xenogen (Caliper Company). Human umbilical vein endothelial cells (HUVEC) and cancer-associated fibroblast (CAF) lines were obtained from Clonetics Corp. and Asterand, respectively. The anti-cleaved Notch1 (NICD1), anti-Notch1, CD31, cleaved caspase-3, and γH2AX antibodies were purchased from Cell Signaling Technology. The anti-BrdUrd (bromodeoxyuridine) antibody was obtained from BD Pharmingen.

In vitro cell-based assays

The *in vitro* proliferation assays were carried out by treating exponentially growing cells for 7 days, followed by an MTT assay to measure cell viability. Real-time measurement of cell migration was done using the CIM-Plate 16 package (Roche Applied Science) according to the manufacturer's instructions. The rate and onset of cell migration were quantified by an xCELLigence Real-Time Cell Analyzer (Roche Applied Science) for 24 hours.

Mammosphere formation assay

The mammospheres were generated by plating viable cells in 96-well ultra-low attachment plates (Corning) using Mammo Cult complete medium (Stem Technologies) supplemented with 4 μg/mL heparin and 0.5 μg/mL Hydrocortisone. The mammospheres were collected on day 6 and dissociated to yield a single-cell suspension. The treatment effect was evaluated when cells were reseeded for second-generation mammospheres. After a 6-day treatment, the cells were quantified and the images were analyzed using an Olympus 1 × 51 inverted microscope. The *in vitro* angiogenesis tube formation assay was done as previously described (19). For the *ex vivo* mammosphere test, the collected tumors were dissociated into individual cells before carrying out the assay (20). After a 12-day treatment, the images were captured using Cellomics (Thermo Scientific) and quantified using Image-Pro Plus (Media Cybernetics).

In vivo studies and drug administration

All experimental animal procedures conducted internally were carried out in compliance with the Guide for the Care and Use of Laboratory Animals (Institute for Laboratory Animal Research, 1996) and were approved by the Pfizer Global Research and Development Institutional Animal Care and Use Committee. AA0869 is a patient-derived xenograft model and the primary human breast tumor tissue was collected under the UC San Diego IRB-approved protocol with prospective consent. Two million cells or trocar fragment were implanted into the dorsal region of either athymic NCr-nu/nu or severe combined immunodeficient (SCID)-beige mice (Charles River Breeding Laboratories).

Studies using human patient-derived xenograft models, including the HBCX1, HBCX6, HBCX7, HBCX9, HBCX12B, and HBCX17 models, were carried out using athymic nude mice (Harlan Laboratories) at Xentech (France). The studies of BT474 in CB-17 SCID mice (Harlan) and SKBR3

Published OnlineFirst July 17, 2012; DOI: 10.1158/1078-0432.CCR-12-1379

in BALB/c nude mice were conducted at Piedmont Research Lab (Charles River) and Crown Bio, respectively.

To evaluate efficacy, the mice were randomly assigned to different groups when the tumors reached a volume of 100 to 200 mm^3, such that the mean value of the tumor size was matched between the groups. Either vehicle or PF-03084014 was administered orally to mice twice daily for 12 days. Tumor growth inhibition (TGI) was calculated after the treatment ended. Statistical analyses were conducted using GraphPad Prism for one-way ANOVA analysis followed by the Dunnett *t* test ($P < 0.05$ was considered statistically significant).

Pharmacodynamic endpoints assessment

The endogenous levels of NICD1 were assessed either by Western blot or using an ELISA Sandwich Kit (Cell Signaling) according the manufacturer's instructions. The tumors were snap-frozen and pulverized in a liquid nitrogen-cooled mortar before being lysed. For Western blotting, 100 μg of cell or tumor lysates was loaded per lane for analysis.

For functional tumor vasculature assessment, tumor-bearing mice received an intravenous injection of 5 mg/kg fluorescein isothiocyanate (FITC)-lectin (Vector Labs) 15 minutes before euthanasia. The tumor samples were frozen in OCT medium, manually sectioned into 100 μm slices, and stained with anti-CD31 antibody. The fluorescence images were captured using a Nikon Eclipse TE2000 fluorescent microscope with Q-Capture software, and the analysis was carried out using Image Pro Plus 5.1 (Media Cybernetics). For *in vivo* metastasis measurements (21), the tumor-bearing mice were intravenously injected with MMPSense 680 (PerkinElmer, Inc.), twenty-four hours before fluorescence imaging (FMT 2500p; PerkinElmer, Inc.).

RNA isolation

Xenograft tumors were collected and preserved in RNA-later RNA stabilization reagent (Qiagen). RNA was isolated using an RNeasy kit (Qiagen) according to manufacturer's protocol with an additional DNA digestion step. The RNA concentration and integrity were measured using a Nano-Drop (Thermo Fisher Scientific) and a 2100 Bioanalyzer (Agilent Technologies), respectively.

nCounter gene expression assay

nCounter probes were designed and obtained from NanoString Technologies. The human probe sequences, which are listed in Supplementary Table S1, were screened against mouse RefSeq to eliminate potentially cross-hybridizing probes. Each assay was carried out using at least 2 biologic replicates. Total RNA (100 ng) was hybridized to nCounter capture and reporter probes at 65°C for 16 hours. The hybridized products were purified and processed using an automated sample prep station, and the images were prepared using the NanoString Digital Analyzer according to the company's standard gene expression assay protocol [http://www.NanoString.com].

nCounter data analysis

The counts were first normalized to 6 spiked-in positive controls to correct for experimental variability. A reference normalization factor was determined by first calculating the geometric mean of the positive controls for each sample and then computing the arithmetic mean across all samples. The gene count for each sample was then normalized by dividing by the ratio of the geometric mean of the positive controls for the sample to the reference normalization factor.

To account for the variability in RNA content, the normalized gene counts were further normalized against 4 endogenous control genes. This was carried out by calculating the geometric mean of the endogenous controls for each sample, averaging across all samples, and generating an endogenous normalization factor by computing the ratio of the geometric mean of the endogenous controls to the average value as described above. Each target gene count was divided by this endogenous normalization factor to compute the final normalized target gene count reflective of the transcript level. The detailed gene expression analysis guidelines can be found on the NanoString Technologies website [http://www.NanoString.com]. The final normalized data are available in the Supplementary Table S2, and a detailed sample description is provided in Supplementary Table S3.

Data analysis

Replicates of xenograft mRNA profiling experiments were summarized using median values and $\log_2$ transformed for subsequent analyses. The comparison between tumor growth inhibition and the $\log_2$ vehicle-treated expression values was carried out using the Pearson linear correlation coefficient implemented in R. The analysis of genes modified after PF-03084014 treatment was carried out using the paired moderated *t* statistic in limma (22). Both the nominal *P* values and the *P* values corrected for multiple comparisons using Benjamini and Hochberg's method (23) are shown. All gene expression analyses, figures, and statistical tests were done in R. For reproducibility (24), the input files and the full R code are available in the Supplementary Methods as a Sweave transcript (25).

Results

PF-03084014 impairs Notch pathway signaling in tumor and HUVEC cell lines and results in cellular functional changes

We tested the *in vitro* activity of PF-03084014 against tumor cell proliferation, migration, and self-renewal as well as endothelial cell proliferation and tube formation.

The growth inhibition mediated by PF-03084014 was assessed in a panel of 35 breast cancer cell lines using an MTT assay. In most lines (33 of 35), the 7-day treatment of 2 μmol/L PF-03084014 had no effect. PF-03084014 induced significant growth inhibition exclusively in the HCC1599 ($Notch1^{MUT}$) and MDA-MB-231Luc cell lines after 5 to 7 days of treatment with IC_{50} values of 0.1 and 0.9 μmol/L, respectively. In HUVECs, treatment with PF-03084014 for 7

Published OnlineFirst July 17, 2012; DOI: 10.1158/1078-0432.CCR-12-1379

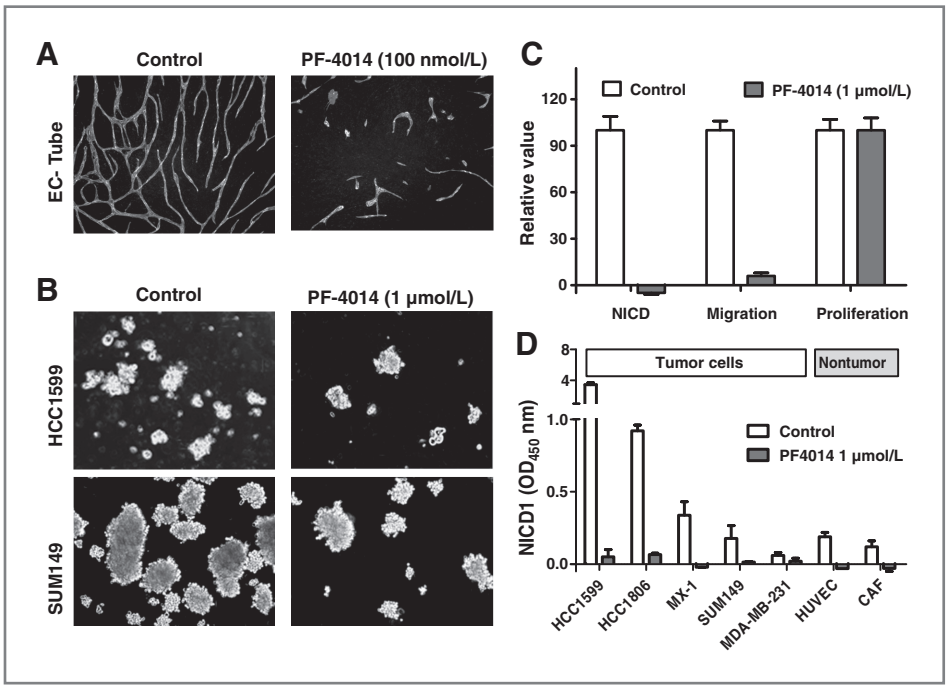

Figure 1. *In vitro* characterization of PF-03084014. A, inhibition of Notch signaling by PF-03084014 (100 nmol/L) blocks HUVEC-fibroblast lumen formation. B, treatment with 1 μmol/L PF-03084014 results in a 50% reduction of nonadherent HCC1599 and SUM149 mammosphere formation. The second-generation mammospheres were generated by plating 500 and 2,000 viable cells per well using SUM149 and HCC1599 cells, respectively, in 96-well ultra low attachment plates (Corning). The imaging analysis was done after a 6-day treatment with PF-03084014. C, in MX1 cells, treatment with 1 μmol/L PF-03084014 leads to a significant suppression of NICD1 and tumor cell migration but fails to exert an antiproliferative effect. D, the decrease in NICD1 levels after treatment with 1 μmol/L PF-03084014 for 48 hours in tumor cells, HUVECs, and CAFs. NICD1 levels were assessed by ELISA. Each data point represents triplicate assays. Value = mean ± SEM.

days reduced cell proliferation with an IC_{50} value of 0.5 μmol/L. To further assess the effect of PF-03084014 against the early steps of angiogenesis, HUVECs were cocultured with human skin fibroblast cells in fibrin gels to generate sprouts with a clear lumen-like structure. The treatment with PF-03084014 for 14 days decreased the lumen formation with an IC_{50} value of 50 nmol/L (Fig. 1A).

The effect of PF-03084014 on the function of tumor-initiating cells was evaluated. Nonadherent mammospheres were established under serum-free conditions. Treatment with 1 μmol/L PF-03084014 reduced mammosphere-forming efficiency by 50% in both HCC1599 and SUM149 cell lines (Fig. 1B), suggesting that the compound inhibits the ability of tumor cells to self-renew. In contrast, PF-03084014 (1 μmol/L) treatment showed no antiproliferative effect in adherent SUM149 cells and 100% cell killing in the HCC1599 cells cultured in serum-containing medium.

The effect of PF-03084014 on tumor cell migration was assessed in MX1 and MDA-MB-231Luc cell lines. Treatment with 1 μmol/L PF-03084014 had no antiproliferative effect in MX1 cells; however, it nevertheless inhibited migration by 95% (Fig. 1C), and a similar result was observed in MDA-MB-231Luc cells.

To confirm the biologic relevance of the functional changes, cells were treated with 1 μmol/L PF-03084014 for 48 hours and then harvested to assess the levels of cleaved Notch1 (NICD1) via ELISA (Fig. 1D). PF-03084014 robustly suppressed NICD1 in HUVECs, CAFs and multiple tumor cell lines, although suppressing NICD1 failed to elicit antiproliferation *in vitro* in several cell lines, including the MX1, HCC1806, and SUM149PT cells.

Diverse mechanisms of PF-03084014–induced antitumor efficacy in breast xenograft models

The dose-dependent antitumor efficacy of PF-03084014 was evaluated in HCC1599 cells. Mice with palpable tumors were administered PF-03084014 p.o. twice daily for 12 days (Fig. 2A). PF-03084014 treatment at 45, 90, and 120 mg/kg resulted in TGI of 95%, 115%, and 120% and a significant growth delay of 20, 30, and 60 days, respectively. Using this dosing schedule, the maximum tolerated dose (MTD) was 120 mg/kg in SCID-bg mice.

To assess the biologic relevance of PF-03084014 treatment *in vivo*, mice bearing HCC1599-derived tumors were treated orally with 120 mg/kg PF-03084014 twice daily, and the tumors were harvested on day 3 for pharmacodynamic assessment. A robust modulation of NICD1 (Fig. 2B) was observed along with significant expression alterations of Notch down stream genes that impact cell cycle and apoptosis, including *MYC*, *CCND1*, *BIRC5*, *CDKN1A*, and *NOXA1* (Fig. 2C). The tumors displayed decreased BrdUrd uptake as well as increased γH2AX and cleaved caspase-3 levels as assayed by immunohistochemistry

Published OnlineFirst July 17, 2012; DOI: 10.1158/1078-0432.CCR-12-1379

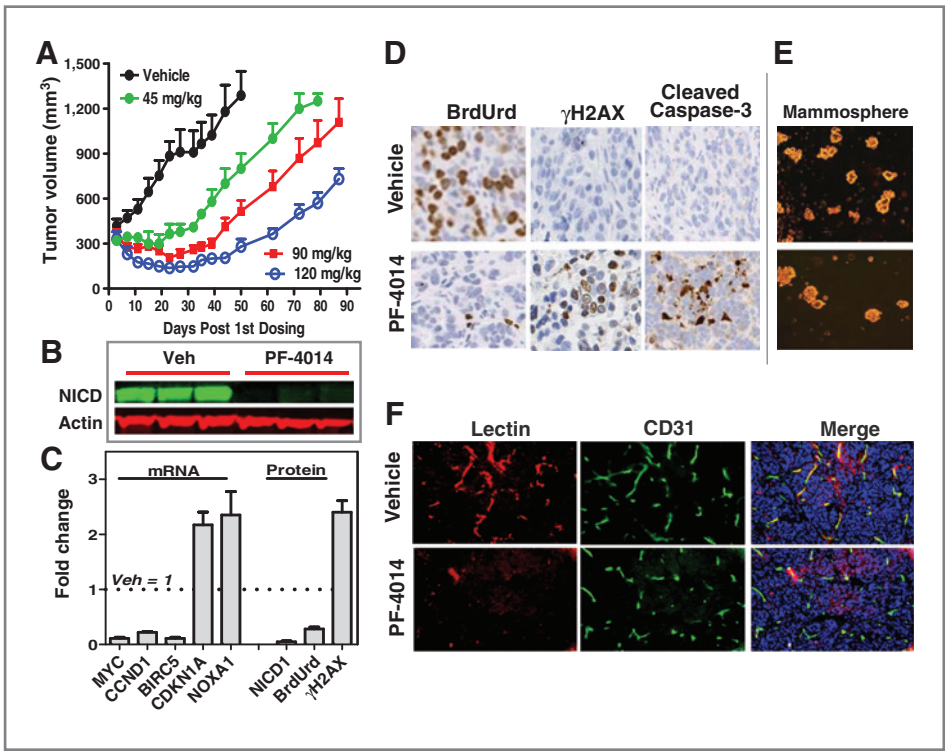

Figure 2. Antitumor efficacy and pharmacodynamic assessment of PF-03084014 in the HCC1599 xenograft model. A, PF-03084014 exhibits dose-dependent antitumor efficacy in a HCC1599 model. Mice bearing palpable tumors were administered PF-03084014 p.o. twice daily at the indicated dose levels for 12 days. $N = 10$ mice per group. B, Western blot measurement of NICD1 expression levels upon treatment. C, the Notch downstream gene modulations correlate with the cell phenotypic changes observed after treatment with PF-03084014. The mRNA expression profile of Notch target genes was normalized to glyceraldehyde-3-phosphate dehydrogenase. The semiquantitative measurement of BrdUrd and yH2AX staining was conducted by a board-certified pathologist. D, the representative staining of BrdUrd, yH2AX, and cleaved caspase-3 in vehicle and treated tumors. Here, 50 mg/kg BrdUrd was administered intraperitoneally to mice 2 hours before harvesting the tumors. The graph represents the value relative to vehicle treatment (= 1). E, treatment of PF-03084014 results in 65% reduction of mammosphere formation. F, PF-03084014 impairs functional vasculature as measured by the lectin perfusion assay. Before tumor collection, mice were injected intravenously with 5 mg/kg FITC-lectin (Vector Labs) 15 minutes before tumor collection. The tumors were collected after the mice were treated with either vehicle or 120 mg/kg PF-03084014 twice daily for 2 days (B, C, D), 12 days (E), and 7 days (F). $N = 5$ mice per group (B, C, D, E, and F). Value = mean ± SEM.

(Fig. 2C and D), suggesting that impairing Notch signaling with PF-03084014 results in antiproliferative activity and induces apoptosis in tumor cells.

The effect of PF-03084014 on the tumor-initiating cells was examined. Treatment with PF-03084014 (120 mg/kg, twice daily) in HCC1599 tumor-bearing mice was carried out for 12 days before tumor harvest. Tumor cells were then dissociated for mammosphere formation assays under stem cell–selective culture conditions. As shown in Fig. 2E, PF-03084014 induced a drastic reduction in mammosphere forming efficiency.

Given the essential role of Notch signaling in vascular development, we assessed whether the efficacy of PF-03084014 was associated with vessel functional change *in vivo*. A fluorescently conjugated FITC-lectin was injected intravenously into HCC1599 tumor-bearing mice after a 7-day continuous treatment. Tumors were harvested for immunofluorescence costaining to assess FITC-lectin and CD31 positivity. PF-03084014 (120 mg/kg) had a minimal impact on CD31-positive endothelial cells, whereas the treated tumors lacked functional lumens as shown by the marked decrease in costaining with FITC-lectin, which indicates the presence of vascular defects (Fig. 2F). Similar results were observed in both the MX1 and MDA-MB-231Luc models.

PF-03084014 displays antimetastasis activity in breast cancer models

The *in vivo* assessment of PF-03084014 against spontaneous metastasis was carried out in MDA-MB-231luc and MX1 mammary fat pad implanted tumor models. Size-matched tumor-bearing mice were administered with PF-03084014 orally twice daily for 12 days. Secondary tumor burden was assessed using an FMT system via injection of MMPsense 680 (Visen) at 24 hours before imaging.

Figure 3A depicts representative fluorescence images of the lung tumor burden in the vehicle- and PF-03084014-treated MX1 mice on day 22 following dosing commencement. On day 23, the lungs were harvested. Hematoxylin and eosin stain (H&E) staining of the lungs revealed marked reductions in the infiltrated tumor foci in PF-03084014-treated groups compared with the vehicle controls, which is

Published OnlineFirst July 17, 2012; DOI: 10.1158/1078-0432.CCR-12-1379

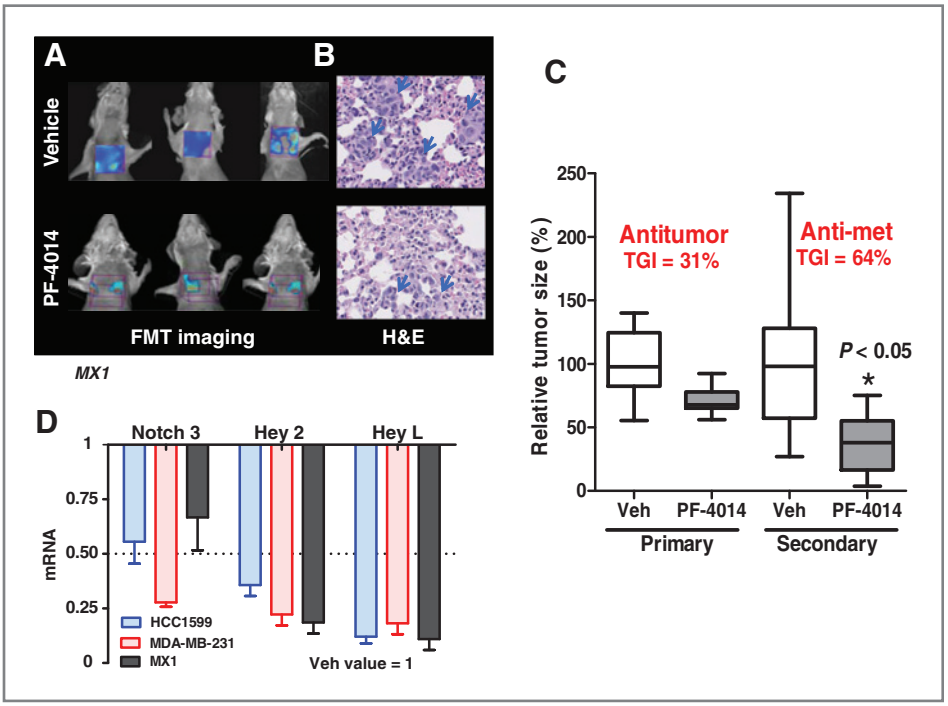

Figure 3. The antitumor and antimetastatic properties of PF-03084014 in the MX1 orthotopic model. Size-matched tumor-bearing mice were administered 90 mg/kg PF-03084014 p.o. twice daily for 12 days. A, representative fluorescence tomographic images of lung metastasis at 22 days after dosing commencement. MX1 tumor–bearing mice received intravenous injections of MMPsense 680 (5 nmol/mouse) 24 hours before analyzing the images using an FMT 2500 system. B, H&E staining of tumor cell infiltration into lungs 24 hours after the FMT imaging analysis. C, PF-03084014 treatment displayed greater antimetastatic efficacy than antitumor efficacy. The primary tumor size under the mammary fat pad was assessed with calipers. $N = 10$ mice per group (A, B, and D); $N = 5$ mice per group (C). Value = mean ± SEM. D, PF-03084014 suppresses stromal Notch target gene expression in multiple models. The tumors were collected after the mice were treated with either vehicle or 120 mg/kg PF-03084014 twice daily for 2 days. The graph represents the value relative to vehicle treatment (= 1).

in agreement with the FMT imaging readout (Fig. 3B). The TGI of PF-03084014 (90 mg/kg) was 31% and 68% in the primary and secondary tumors, respectively (Fig. 3C). Notably, a greater efficacy against tumor cell infiltration into lung than against primary tumor growth was observed in the MX1 model. The antimetastasis activity of PF-03084014 was also observed in the MDA-MB-231luc tumor model.

In solid tumors, aberrant Notch signaling between tumor cells and the host microenvironment was shown to induce neovascularization and metastasis, thus promote disease progression via a noncell autonomous effect (13, 26). In multiple tumor models, including the HCC1599, MX1, and MDA-MB-231Luc models, treatment with PF-03084014 (120 mg/kg, twice daily) for 2 days reduced the expression of the Notch stroma target genes *NOTCH3*, *HEY2*, and *HEYL* (Fig. 3D). The robust decrease in *HeyL* expression is consistent with the antiangiogenic and antimetastatic effects of PF-03084014, as elevated levels of *HeyL* were found in the vasculature of invasive breast carcinomas (27).

PF-03084014 shows antitumor activities in a panel of breast cancer models

The *in vivo* efficacy of PF-03084014 was evaluated in subcutaneously implanted breast cancer xenograft models at or near the MTD level (120 mg/kg). In 10 of the 18 tested breast cancer models (Fig. 4A), PF-03084014 displayed a TGI value of at least 50% ($P < 0.05$). Interestingly, the *in vivo* sensitivity (TGI > 50%) of PF-03084014 in breast cancer models did not correlate with the 7-day proliferation assay (MTT) results (Fig. 4B), in which PF-03084014 only inhibited the growth of the HCC1599 and MDA-MB-231Luc cultures with IC_{50} values of 0.1 and 0.9 μmol/L, respectively. The disconnect between the *in vitro* and *in vivo* efficacies is not simply due to differences in exposure as the highest concentration of PF-03084014 tested in the *in vitro* antiproliferation assay (2 μmol/L) exceeded the steady-state concentration achieved *in vivo* (1.2 μmol/L) at the MTD.

Using an ELISA assay, we assessed the baseline expression levels of the Notch1 intracellular domain as a marker of Notch pathway activation; NICD1 levels did not vary significantly between the sensitive and resistant tumors (Fig. 4C). We were unable to develop assays for NICD2, NICD3, and NICD4 because of the limited supply of commercially available antibodies; therefore, we used a different biomarker approach to predict sensitivity to PF-03084014.

The NICD1 levels in the $Notch1^{mut}$ HCC1599 cells were relatively high both *in vitro* and *in vivo*. In contrast, NICD1 was below the detection limit *in vitro* in the MDA-MB-361, MDA-MB-231, and MDA-MB-436 cell lines, whereas it was significantly elevated in the corresponding *in vivo* tumors (Fig. 4D). These results suggested that because of the

Published OnlineFirst July 17, 2012; DOI: 10.1158/1078-0432.CCR-12-1379

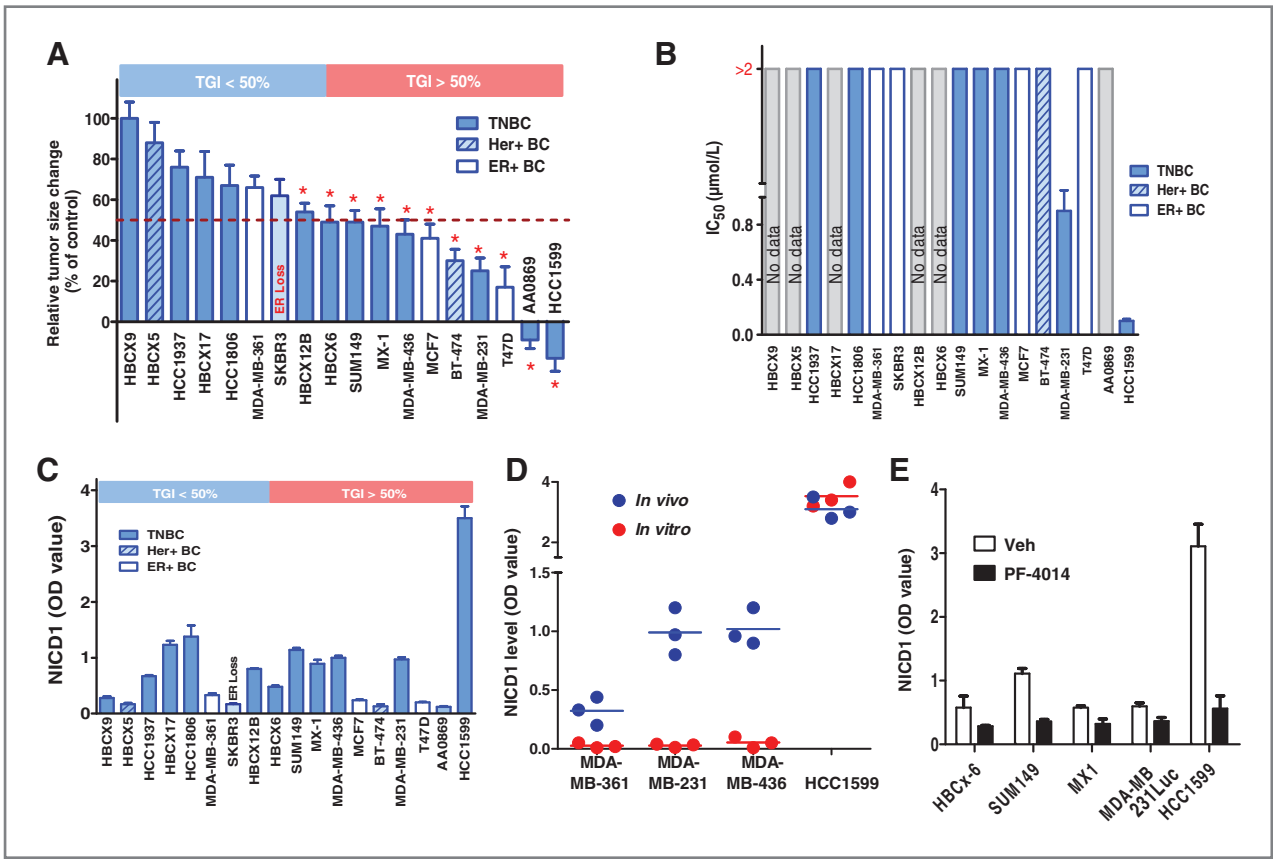

Figure 4. The antitumor efficacy of PF-03084014 in breast cancer cells and xenograft models. A, the effect of PF-03084014 on tumor growth in a panel of breast cancer xenografts. Size-matched tumor-bearing mice were administered 120 mg/kg PF-03084014 p.o. twice daily for 12 days. The relative tumor size change = 100*ΔT/ΔC. The ΔC (ΔT) value was measured by subtracting the mean tumor volume for the vehicle (treated) group on the first day of treatment from the mean tumor volume on the evaluation day. The relative tumor size changes were assessed after the treatment ended. *, $P < 0.05$. B, in an MTT assay, 2 μmol/L PF-03084014 treatment for 7 days displayed no antiproliferative activity in most of the breast cancer cell lines. C, the baseline NICD1 levels were variable across different breast cancer models. D, the differences in NICD1 levels between the *in vitro* and *in vivo* settings suggest the activation of Notch1 signaling by the *in vivo* microenvironment (loaded 100 μg protein). E, treatment with 120 mg/kg PF-03084014 for 2 days led to a decrease in NICD1 levels in the efficacious tumor models. NICD1 levels were assayed by ELISA.

stroma-activated Notch signaling, PF-03084014 was significantly more active *in vivo*.

In a subset of responding tumor models (TGI > 50%) with high baseline levels of NICD1, pharmacodynamic studies were carried out. Tumor-bearing mice were treated with 120 mg/kg PF-03084014 twice daily for 2 days, and the tumors were harvested on the third day for NICD1 analysis. Treatment with PF-03084014 suppressed NICD1 (Fig. 4E), suggesting that PF-03084014 efficacy is in part mediated by the blockade of Notch1 signaling.

Expression of Notch pathway target genes corresponds to the response to PF-03084014 *in vivo*

To establish the correlation of the PF-03084014-induced efficacy with Notch pathway biomarkers in 17 *in vivo* models, we analyzed the expression of 40 genes selected primarily from the Notch pathway, including receptors, ligands, and regulators such as *NUMB*, as well as canonical target genes such as the *Hes* and *Hey* gene families. We also selected cell-cycle genes associated with the Notch pathway (28). In total, 45 probes from 40 genes were profiled using NanoString technology.

We first analyzed the correlation between the vehicle-treated gene expression profiles and the PF-03084014 *in vivo* activity. The expression of 11 probes from 8 genes positively correlated with tumor growth inhibition at the nominal *P* less than 0.05 (Fig. 5A). The most significant genes included the 3 canonical Notch pathway targets, *HEY2*, *HES4*, and *HES3* [correlated at nominal $P < 0.01$ and a false discovery rate (FDR) adjusted $P < 0.15$]. *NOTCH2* represented the only Notch receptor expression profile that significantly correlated with compound activity; the expression of the other 3 notch receptors, *NOTCH1*, *NOTCH3*, and *NOTCH4*, did not significantly correlate with response. We also identified 4 unique genes, *CDKN1B*, *HEYL*, *DTX1*, and *CDKN1A*, with which the expression negatively correlated with PF-03084014 activity (defined $R < -0.1$), although none of these correlations was significant. In addition to the correlation tests, we also carried out differential gene expression analysis between the most sensitive (defined by TGI > 70%)

Published OnlineFirst July 17, 2012; DOI: 10.1158/1078-0432.CCR-12-1379

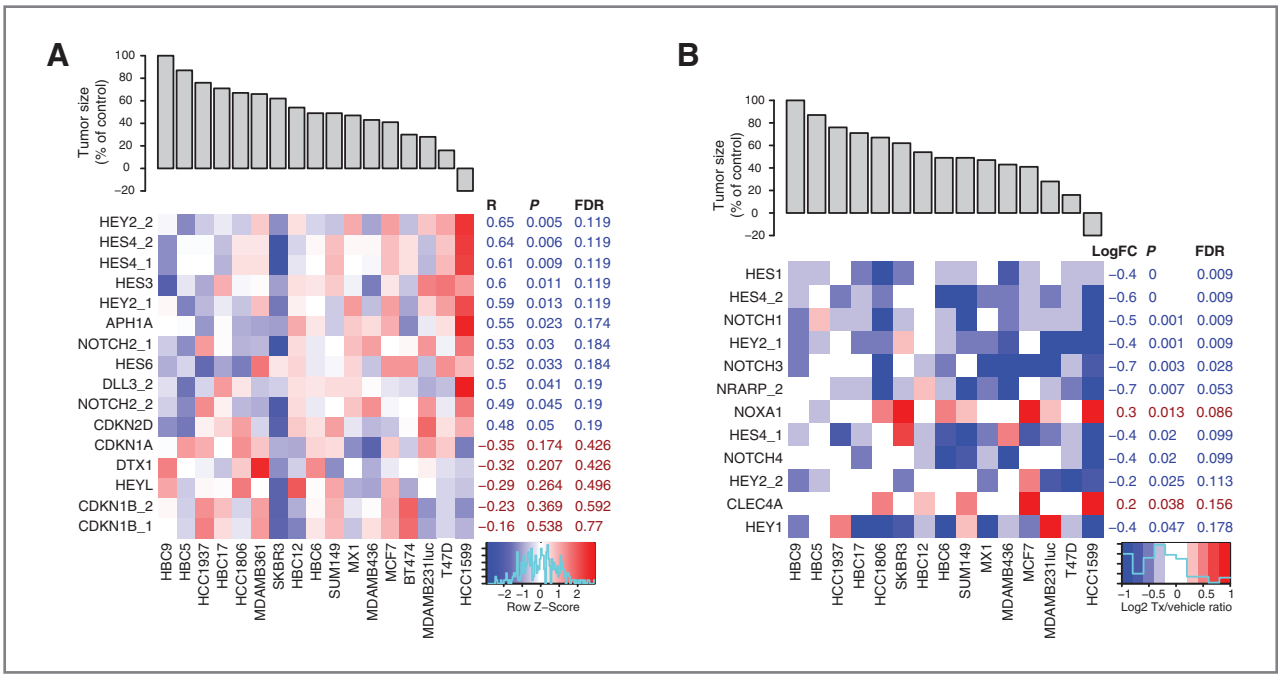

Figure 5. Gene expression correlated with PF-03084014 sensitivity and treatment modulation. A, top genes with baseline expression correlated with tumor growth inhibition. Vehicle-treated expression levels were taken as a baseline and compared with antitumor efficacy. Samples were sorted from most resistant on the left to most sensitive on the right (top). The heat map (bottom) shows relative baseline expression of each gene; red means that gene is overexpressed compared with average in a given sample, blue underexpressed. On the top are genes most significantly overexpressed in sensitive models; the bottom 5 genes are negatively correlated ($R < -0.1$) with sensitivity. The panel on the right shows the linear correlation coefficient (R) between tumor inhibition and expression values, the corresponding nominal *P* value and Benjamini and Hochberg's corrected *P* values (FDR). Genes with positive R values (up in sensitive models) are highlighted in blue, and the 5 genes negatively correlated with sensitivity are in red. B, expression modulation after PF-03084014 treatment compared with vehicle-treated samples. Samples were again sorted from resistant on the left to sensitive on the right (top). The heat map shows relative expression modulation of each gene; red means that gene is overexpressed post PF-03084014 treatment compared with the vehicle control, blue downregulated by the PF-03084014 treatment. The panel on the right shows $\log_2$ of fold change (LogFC) between PF-03084014 and vehicle-treated samples, moderated *t* test statistics *P* values and Benjamini and Hochberg's corrected *P* values (FDR). Genes highlighted in blue are significantly downregulated posttreatment across the panel of models; the 2 red rows correspond to mRNAs upregulated after PF-03084014 treatment.

and resistant (models with TGI < 30%) models. This analysis (Supplementary Fig. S1 and Supplementary Methods) confirmed that *HEY2* was the most significantly upregulated gene and that *CDKN1B* was the most significantly downregulated gene in the most sensitive models.

Next, we analyzed the modulation of the 40 selected genes after treatment. For 15 *in vivo* models, we assessed the modulation upon PF-03084014 treatment compared with vehicle treatment. In both cases, RNA was collected 2 days after treatment and profiled using the NanoString assay. We identified 12 different probes from 10 unique genes that were significantly modulated upon PF-03084014 treatment (univariate $P < 0.05$, paired *t* test) as shown in Fig. 5B. The most significant genes (nominal $P < 0.001$) were *HES1*, *HES4*, *NOTCH1*, and *HEY2*. A majority of the significantly modulated genes were downregulated upon treatment, including several canonical Notch pathway targets (*HES*, *HES4*, *HEY2*, *NRARP*, and *HEY1*) and the 3 Notch receptors, *NOTCH1*, *NOTCH3*, and *NOTCH4*. Interestingly, high baseline levels of *HES4* and *HEY2* expression correlate with efficacy, and these genes are among the most downregulated mRNAs posttreatment. *NOXA1* and *CLEC4A* were the only genes that were significantly upregulated after treatment.

The HCC1599 model was the only model in which PF-03084014 treatment led to tumor regression. Therefore, we investigated the genes that were differentially expressed between the HCC1599 model and the other models to characterize the treatment-induced molecular changes in HCC1599 cells (Supplementary Fig. S2A). Several genes, many of which represented cell cycle and/or apoptosis factors, differed significantly in the magnitude of modulation; *MYC*, *BIRC5*/survivin, and *CCND1*/cyclin D1 were downregulated more than 4-fold ($\log_2$ fold change < -2) posttreatment in the HCC1599 model compared with other models. Unsupervised clustering of all assayed cell-cycle genes revealed a distinct modulation pattern in HCC1599 cells (Supplementary Fig. S2B).

We also compared the magnitude of mRNA modulation after treatment with the baseline gene expression levels and the antitumor efficacy. Table 1A lists the mRNAs for which the extent of posttreatment modulation correlated with the baseline expression levels in vehicle-treated samples (for more details, see Supplementary Fig. S3). In all of the significant cases, there was a negative correlation between the baseline expression level and the magnitude of modulation. In other words, the higher the relative expression

Published OnlineFirst July 17, 2012; DOI: 10.1158/1078-0432.CCR-12-1379

Table 1. The Notch target gene analyses and the biomarker identifications of PF-03084014 in breast cancer xenograft models

Gene	Pearson R	*P*	FDR adjusted *P*[a]
Correlation between gene modulation after treatment and baseline expression (A)			
HES4_2	–0.72	0.002	0.053
HES4_1	–0.72	0.002	0.053
NRARP_1	–0.67	0.006	0.060
DLL3_1	–0.67	0.007	0.060
HES3	–0.67	0.007	0.060
DTX1	–0.61	0.015	0.112
PTCRA	–0.56	0.030	0.139
CDKN2D	–0.56	0.030	0.139
Hey2_1	–0.56	0.030	0.139
CDKN1B_1	–0.56	0.031	0.139
DLL3_2	–0.46	0.087	0.356
NRARP_2	–0.45	0.096	0.359
Correlation between modulation after treatment and TGI (B)			
Notch4	0.67	0.006	0.092
NCSTN	–0.66	0.008	0.092
NRARP_1	0.65	0.009	0.092
NRARP_2	0.64	0.010	0.092
HES4_2	0.63	0.011	0.092
CDKN1B_2	–0.63	0.012	0.092
DLL3_2	0.62	0.014	0.093
Hey2_1	0.60	0.019	0.106
BIRC5	0.58	0.024	0.108
HES6	0.57	0.026	0.108
MYC	0.57	0.026	0.108
CCND1	0.55	0.033	0.124
HES4_1	0.52	0.045	0.155
FURIN	–0.52	0.049	0.158
Jag1	0.51	0.054	0.159
Notch2_1	–0.49	0.061	0.159
PTCRA	0.49	0.063	0.159
NOXA1	–0.49	0.065	0.159
CLEC4A	–0.48	0.067	0.159
Notch2_2	–0.47	0.076	0.170
NUMB	–0.46	0.085	0.182

[a]Benjamini and Hochberg's correction.

level of a gene, the more it was downregulated after treatment (for downregulated genes) or the less it is upregulated (for upregulated genes). The genes that were downregulated by treatment with GSI include the Notch target genes *HES4*, *NRARP*, *HES3*, and *HEY2*. In contrast, the models with low baseline *CDKN1B* expression, which are sensitive to PF-03084014, displayed *CDKN1B* upregulation upon treatment. We found that following treatment with PF-03084014, the Notch target genes of the *Hes* and *Hey* families were downregulated, whereas the negative regulator *CDKN1B* was upregulated, and the changes were more pronounced in the sensitive models. Table 1B and Supplementary Fig. S4 show the genes for which the magnitude of modulation after treatment correlated with the antitumor efficacy. Strong downregulation of several genes, including *NOTCH4*, *NRARP*, *HES4*, *DLL3*, and *HEY2* was associated with increased tumor inhibition as was the upregulation of *NCSTN* and *CDKN1B*.

Discussion

In this article, we examine the preclinical properties of PF-03084014, a GSI, in breast cancer cell lines and breast cancer models. PF-03084014 impairs the Notch pathway and shows antitumor and antimetastasis activities. Using a panel of breast xenograft models, we investigated different biomarker approaches for patient stratification and proof-of-mechanism. This work provides insight into the mechanism of PF-03084014 activity and may potentially aid the clinical development in breast cancer patients.

Treatment with PF-03084014 *in vivo* resulted in antitumor activity (TGI > 50%) in 10 of the 18 breast xenograft models. These results did not correlate with the *in vitro* growth inhibition assay using the corresponding cell lines, despite the modulation of NICD1 levels by PF-03084014 in many of the cell lines. Among the 12 evaluable cell lines, only 2 displayed growth inhibition following treatment with 2 μmol/L PF-03084014, which represents a concentration above the steady-state plasma concentration (C_{ss} = 1.2 μmol/L) at the *in vivo* MTD. One of these cell lines was the HCC1599, which harbors an activating *NOTCH1* mutation (3), and was highly responsive to PF-03084014 treatment in both *in vitro* and *in vivo* conditions. *NOTCH1* and *NOTCH2* gene rearrangements have recently been reported in ER-negative breast tumors and cell lines (3). Cell lines with Notch fusions that retain the γ-secretase cleavage site are sensitive to GSI. In addition, we also observed PF-03084014–induced antitumor efficacy in other ER-positive models, thereby suggesting that the GSI responsive population in breast cancer is not restricted to ER-negative patients or those with *NOTCH* gene fusions.

Notch signaling mediates breast cancer disease progression via both cell-autonomous and nonautonomous interactions. We observed elevated NICD1 levels in some of the GSI-responding models *in vivo* compared with the corresponding cell lines in culture, suggesting that the absence of a stromal compartment may be responsible for the overall lack of the *in vitro* antiproliferative activity of PF-03084014. In agreement with previous reports, the Notch pathway activation in solid tumors often depends on ligand–receptor interactions via tumor and stroma cell-to-cell contact (5).

Biomarkers were assessed by correlating the *in vivo* TGI with the mRNA expression of Notch pathway genes. We profiled both the baseline (estimated by vehicle-treated profiles) and posttreatment expression of 40 selected pathway genes. Given the relatively modest number of models, we focused on a small set of genes to mitigate the risk of

Published OnlineFirst July 17, 2012; DOI: 10.1158/1078-0432.CCR-12-1379

overfitting. This hypothesis-driven approach revealed that neither expression of Notch receptors nor their ligands significantly correlated with PF-03084014–induced antitumor activity with the possible exception of *NOTCH2*, whereas the expression of several Notch pathway target genes, including *HEY2*, *HES4* and *HES3*, clearly correlated with increased sensitivity to the inhibitor. These 3 genes were also significantly downregulated after treatment. Interestingly, the baseline expression of the most significantly modulated gene, *HES1*, failed to correlate with the compound sensitivity results *in vivo*. Our results suggest that the expression of select downstream Notch pathway targets better reflects the overall status of pathway activation than the Notch receptors and, in turn, sensitivity to GSIs. Similar results have been previously reported for other GSIs (28). The lack of a correlation between PF-03084014 activity and the mRNA expression of the Notch receptors and ligands may be due to exclusive activation of the Notch receptors and/or the posttranscriptional regulation of the proteins.

It has been previously reported (28) that a 10-gene Notch signature score corresponds with the response to the GSI, MRK-003, in T-cell acute lymphoblastic leukemia (T-ALL) cells. The 10-gene Notch score predicted PF-03084014 activity in our *in vivo* breast cancer models, albeit with borderline significance ($P = 0.05$; Supplementary Fig. 5S). Two of the predictive markers that we identified, *HEY2* and *HES4*, along with 2 genes significantly modulated by PF-03084014, *HES1*, and *NRAPR* were among the 10 Notch pathway targets reported (28). These results suggest that although the biologic processes associated with GSI sensitivity are similar and linked to the activation of downstream Notch signaling, the expression of key effector genes may differ between different tissues. For certain genes, the magnitude of expression modulation after short-term treatment correlates with the subsequent antitumor efficacy of PF-03084014 during long-term treatment. One can speculate that the expression changes of these genes after the initial dose may represent the early readout of PF-03084014 efficacy in breast tumors; this hypothesis would require confirmation in independent samples.

PF-03084014 reduced proliferation and induced apoptosis in the HCC1599 ($Notch1^{mut}$) model in a dose-dependent manner, and the efficacy significantly correlated with the depletion of NICD1, thus suggesting that the efficacy was driven at least in part by Notch1 pathway impairment. Consistently, we observed a robust treatment-induced modulation of Notch down stream genes that are associated with cell cycle and apoptosis, including *MYC*, *CCND1*, *BIRC5*, and *NOXA1*, which may be due to pan-Notch inhibition by PF-03084014.

Notch is one of the signaling pathways that mediates breast cancer cell self-renew (29). The *in vivo* efficacy of PF-030841014 may be partly derived from the reduction of tumor-initiating cells. Indeed, PF-03084014 significantly suppressed mammosphere formation efficiency in HCC1599 residual tumor cells after a 12-day treatment period *in vivo*. An *in vitro* mammosphere formation assay using HCC1599 and SUM149 cells also confirmed the ability of PF-03084014 against tumor cell self-renewal. For both SUM149 and HCC1599 cells, PF-030841014 triggered differential responses against cell growth and maintenance under high- and low-serum conditions. This maybe explained by that the signaling pathways for regulating differentiated cell to proliferate are not necessarily same as those for cancer stem cell self-renewal.

PF-03084014 also caused less functional vasculature *in vivo* at a high dose level (120 mg/kg) as displayed with a lectin perfusion assay. However, the changes in CD31 staining were marginal, which could be a net outcome of concurrent suppression in Dll4- and Jagged 1-mediated angiogenesis, as Jagged 1 and Dll4 exert opposing effects on endothelial cells, and blocking either pathway would yield less functional tumor vasculature (9). A decrease in endothelial cell proliferation has also been reported using other GSIs (30). In contrast to an anti-VEGF inhibitor, PF-03084014 only impaired tumor vasculature at a high dose level (>100 mg/kg), whereas target-associated efficacy was observed at a much lower dose (45 mg/kg). These results indicate that the antiangiogenic effect is not a dominant mechanism responsible for the therapeutic response to PF-03084014 in breast cancer.

In PF-03084014-treated MX1 tumor-bearing mice, we observed higher levels of antimetastatic activity than antitumor efficacy. *In vitro*, 1 μmol/L PF-03084014 inhibited MX1 cell migration by 95% but failed to exert any growth inhibitory effect. When primary tumor cells disseminate to distant organs, secondary tumor formation requires both a malignant cell with high invasive and migratory capabilities and a permissive microenvironment, in which the tumor cell interacts with nearby stromal cells to establish a secondary tumor. Notch signaling is implicated throughout this metastatic cascade via EMT (31, 32), TGF-β signaling (13), neovascularization, and other mechanisms. In addition to the treatment-induced decrease of tumor cell motility, impairing Notch signaling in the stromal compartment may also contribute to the antimetastatic activity of PF-03084014. Supporting this notion, cell-autonomous Notch signaling was modulated by PF-03084014 in cultured HUVECs and CAFs. *In vivo*, PF-03084014 treatment led to a marked decrease in the expression of the stromal gene, *HEYL*, a Notch target gene that is highly expressed in invasive breast cancer vasculature and drives neovascularization (27). Notably, PF-03084014–induced modulation of *HEYL* expression was not observed in HUVEC culture *in vitro*. These results highlight the potential therapeutic uses of PF-03084014 to combat both primary tumor growth and tumor metastasis to distant sites.

As breast orthotopic models rarely develop efficient metastases, we were unable to generate sufficient data to draw a correlation between the antimetastatic effect and Notch pathway biomarkers. One of the caveats of using TGI as an endpoint to generate predictive biomarkers is that primary tumor growth may not necessarily reflect comprehensive human disease progression, as clinical metastases account for a large percentage of breast cancer-associated deaths. Another limitation of xenograft-derived biomarkers

Published OnlineFirst July 17, 2012; DOI: 10.1158/1078-0432.CCR-12-1379

is that aberrant Notch signaling can occur between the tumor–stroma cell interactions, whereas the mouse stromal microenvironment may not fully recapitulate the situation in patient tumors.

Taken together, these data highlight that PF-03084014 exhibits efficacy against breast tumor growth and metastasis through pleiotropic mechanism. In a panel of breast xenografts, we identified a Notch gene signature that is predictive of the sensitivity to PF-03084014. This gene signature could serve as a biomarker for patient stratification and aid in personalized therapeutic treatment strategies for PF-03084014. In recent years, a large body of evidence has shown that Notch signaling cross-talks with many other oncogenic pathways to drive cancer progression. Future work is warranted to identify a rational combination strategy to reach the full potential for the clinical development of PF-03084014.

Disclosure of Potential Conflicts of Interest

All authors are either current or former employees of Pfizer. C.C. Zhang has been Principle Scientist at Pfizer. J.G. Christensen has been Sr. Director and has ownership interest (including patents) in Pfizer, Inc. No other potential conflicts of interest were disclosed.

Authors' Contributions

Conception and design: C.C. Zhang, A. Pavlicek, M.E. Lira, X. Zheng, Q. Zong, T. Smeal, J.G. Christensen
Development of methodology: Q. Zhang, M.E. Lira, X. Zheng, M. Ozeck, Q. Zong, P.B. Lappin, A. Wong
Acquisition of data (provided animals, acquired and managed patients, provided facilities, etc.): C.C. Zhang, Q. Zhang, C.L. Painter, Z. Yan, N.V. Lee, M. Ozeck, M. Qiu, P.B. Lappin
Analysis and interpretation of data (e.g., statistical analysis, biostatistics, computational analysis): C.C. Zhang, A. Pavlicek, C.L. Painter, M. Ozeck, Q. Zong, P.B. Lappin, P.A. Rejto, T. Smeal, J.G. Christensen
Writing, review, and/or revision of the manuscript: C.C. Zhang, A. Pavlicek, C.L. Painter, P.B. Lappin, P.A. Rejto, J.G. Christensen
Administrative, technical, or material support (i.e., reporting or organizing data, constructing databases): Q. Zhang, C.L. Painter
Study supervision: C.C. Zhang, X. Zheng

Acknowledgments

The authors thank Stephanie Shi for assisting all the external studies and also Chassidy Hall (Piedmont Research Center), Yanmei Sun (Crown Bioscience), Myriam Lassalle (XenTech), Truong-An Tran (XenTech), and Jean-Gabriel Judde (XenTech) for conducting the external *in vivo* xenograft studies.

The costs of publication of this article were defrayed in part by the payment of page charges. This article must therefore be hereby marked *advertisement* in accordance with 18 U.S.C. Section 1734 solely to indicate this fact.

Received April 30, 2012; revised June 30, 2012; accepted July 9, 2012; published OnlineFirst July 17, 2012.

References

1. Dickson BC, Mulligan AM, Zhang H, Lockwood G, O'Malley FP, Egan SE, et al. High-level JAG1 mRNA and protein predict poor outcome in breast cancer. Mod Pathol 2007;20:685–93.
2. Reedijk M, Odorcic S, Chang L, Zhang H, Miller N, McCready DR. High-level coexpression of JAG1 and NOTCH1 is observed in human breast cancer and is associated with poor overall survival. Cancer Res 2005;65:8530–7.
3. Robinson DR, Kalyana-Sundaram S, Wu Y-M, Shankar S, Cao X, Ateeq B, et al. Functionally recurrent rearrangements of the MAST kinase and Notch gene families in breast cancer. Nat Med 2011;17:1646–51.
4. Pece S, Serresi M, Santolini E, Capra M, Hulleman E, Galimberti V. Loss of negative regulation by Numb over Notch is relevant to human breast carcinogenesis. J Cell Biol 2004;167:215–21.
5. Ranganathan P, Weaver KL, Capobianco AJ. Notch signalling in solid tumours: a little bit of everything but not all the time. Nat Rev Cancer 2011;11:338–51.
6. Schwanbeck R, Martini S, Bernoth K, Just U. The Notch signaling pathway: Molecular basis of cell context dependency. Eur J Cell Biol 2011;90:572–81.
7. Claxton S, Fruttiger M. Periodic Delta-like 4 expression in developing retinal arteries. Gene Expr Patterns 2004;5:123–7.
8. Ridgway J, Zhang G, Wu Y, Stawicki S, Liang WC, Chanthery Y, et al. Inhibition of Dll4 signalling inhibits tumour growth by deregulating angiogenesis. Nature 2006;444:1083–7.
9. Benedito R, Roca C, Sörensen I, Adams S, Gossler A, Fruttiger M, et al. The notch ligands Dll4 and Jagged1 have opposing effects on angiogenesis. Cell 2009;137:1124–35.
10. Zeng Q, Li S, Chepeha DB, Giordano TJ, Li J, Zhang H. Crosstalk between tumor and endothelial cells promotes tumor angiogenesis by MAPK activation of Notch signaling. Cancer Cell 2005;8:13–23.
11. Mikhailik A, Mazella J, Liang S, Tseng L. Notch ligand-dependent gene expression in human endometrial stromal cells. Biochem Biophys Res Commun 2009;388:479–82.
12. Sweeney C, Morrow D, Birney YA, Coyle S, Hennessy C, Scheller A, et al. Notch 1 and 3 receptors modulate vascular smooth muscle cell growth, apoptosis and migration via a CBF-1/RBP-Jk dependent pathway. FASEB J 2004;18:1421–3.
13. Sethi N, Dai X, Winter CG, Kang Y. Tumor-derived Jagged1 promotes osteolytic bone metastasis of breast cancer by engaging notch signaling in bone cells. Cancer Cell 2011;19:192–205.
14. Al-Husaini H, Subramanyam D, Reedijk MJ, Sridhar SS. Notch signaling pathway as a therapeutic target in breast cancer. Mol Cancer Ther 2011;10:9–15.
15. Hoey T, Yen WC, Axelrod F, Basi J, Donigian L, Dylla S, et al. DLL4 blockade inhibits tumor growth and reduces tumor-initiating cell frequency. Cell Stem Cell 2009;5:168–77.
16. Luistro L, He W, Smith M, Packman K, Vilenchik M, Carvajal D, et al. Preclinical profile of a potent γ-secretase inhibitor targeting notch signaling with *in vivo* efficacy and pharmacodynamic properties. Cancer Res 2009;69:7672–80.
17. Konishi J, Kawaguchi KS, Vo H, Haruki N, Gonzalez A, Carbone DP, et al. γ-Secretase inhibitor prevents notch3 activation and reduces proliferation in human lung cancers. Cancer Res 2007;67:8051–7.
18. Wei P, Walls M, Qiu M, Ding R, Denlinger RH, Wong A, et al. Evaluation of selective γ-secretase inhibitor PF-03084014 for its antitumor efficacy and gastrointestinal safety to guide optimal clinical trial design. Mol Cancer Ther 2010;9:1618–28.
19. Donovan D, Brown NJ, Bishop ET, Lewis CE. Comparison of three *in vitro* human 'angiogenesis' assays with capillaries formed *in vivo*. Angiogenesis 2001;4:113–21.
20. Hwang-Verslues WW, Kuo W-H, Chang P-H, Pan C-C, Wang H-H, Tsai S-T, et al. Multiple lineages of human breast cancer stem/progenitor cells identified by profiling with stem cell markers. PLoS One 2009;4:e8377.
21. Grimm J, Kirsch DG, Windsor SD, Kim CF, Santiago PM, Ntziachristos V, et al. Use of gene expression profiling to direct *in vivo* molecular imaging of lung cancer. Proc Natl Acad Sci U S A 2005;102:14404–9.
22. Smyth GK. Limma: linear models for microarray data In:Gentleman R, Carey V, Dudoit S, Irizarry R, Huber W, editors. Bioinformatics and computational biology solutions using R and bioconductor. New York: Springer; 2005:397–420.
23. Benjamini Y, Hochberg Y. Controlling the false discovery rate: a practical and powerful approach to multiple testing. J R Stat Soc Series B (Methodological) 1995;57:289–300.

Published OnlineFirst July 17, 2012; DOI: 10.1158/1078-0432.CCR-12-1379

24. Gentleman R. Reproducible Research: A Bioinformatics case study. Stat Appl Genet Mol 2005;4: Article 2.
25. Leisch F. Sweave: Dynamic generation of statistical reports using literate data analysis. In:Härdle W, Rönz B, editors. Proceedings in Computational Statistics. Berlin, Germany: Springer Compstat 2002: 575–80.
26. Li J-L, Harris AL. Notch signaling from tumor cells: A new mechanism of angiogenesis. Cancer Cell 2005;8:1–3.
27. Parker BS, Argani P, Cook BP, Liangfeng H, Chartrand SD, Zhang M, et al. Alterations in vascular gene expression in invasive breast carcinoma. Cancer Res 2004;64:7857–66.
28. Rao SS, O'Neil J, Liberator CD, Hardwick JS, Dai X, Zhang T, et al. Inhibition of NOTCH signaling by gamma secretase inhibitor engages the RB pathway and elicits cell cycle exit in T-cell acute lymphoblastic leukemia cells. Cancer Res 2009;69:3060–8.
29. Korkaya H, Liu S, Wicha MS. Breast cancer stem cells, cytokine networks, and the tumor microenvironment. J Clin Invest 2011;121: 3804–9.
30. Paris D, Quadros A, Patel N, DelleDonne A, Humphrey J, Mullan M. Inhibition of angiogenesis and tumor growth by [beta] and [gamma]-secretase inhibitors. Eur J Pharmacol 2005;514: 1–15.
31. Leong KG, Niessen K, Kulic I, Raouf A, Eaves C, Pollet I, et al. Jagged1-mediated Notch activation induces epithelial-to-mesenchymal transition through Slug-induced repression of E-cadherin. J Exp Med 2007;204:2935–48.
32. Yang Y, Ahn YH, Gibbons DL, Zang Y, Lin W, Thilaganathan N, et al. The Notch ligand Jagged2 promotes lung adenocarcinoma metastasis through a miR-200–dependent pathway in mice. J Clin Invest 2011; 121:1373–85.

Published OnlineFirst July 17, 2012; DOI: 10.1158/1078-0432.CCR-12-1379

Clinical Cancer Research

Biomarker and Pharmacologic Evaluation of the γ-Secretase Inhibitor PF-03084014 in Breast Cancer Models

Cathy C. Zhang, Adam Pavlicek, Qin Zhang, et al.

Clin Cancer Res Published OnlineFirst July 17, 2012.